

Effects of Weld Heat Input on Mechanical Characteristics of Low Carbon Sheet Steels

Sait Ozmen ERUSLU*, Ismail Berk AKBULUT**, Ibrahim Savas DALMIS***

*Tekirdağ Namık Kemal University, Çorlu Faculty of Engineering, Mechanical Engineering Department, 59860, Çorlu-Tekirdağ, Türkiye, E-mail: oeruslu@nku.edu.tr

**Tekirdağ Namık Kemal University, Çorlu Faculty of Engineering, Mechanical Engineering Department, 59860, Çorlu-Tekirdağ, Türkiye, E-mail: Ismail-Berk.Akbulut@bshg.com

***Tekirdağ Namık Kemal University, Çorlu Faculty of Engineering, Mechanical Engineering Department, 59860, Çorlu-Tekirdağ, Türkiye, E-mail: idalmis@nku.edu.tr (Corresponding author)

<https://doi.org/10.5755/j02.mech.34356>

1. Introduction

Welding is a widely utilized process in the manufacturing industry with various applications such as joining, line heating, cladding, etc. Welding heat is used for thick plates in forming process that involves shaping steel plates into curved forms using heat generated from weld lines. This technique is typically applied with the aid of an appropriate heat source for thermal forming, ensuring that the heating does not surpass the recrystallization temperature of the materials [1].

One of the commonly employed heat sources for weld heating is the oxyfuel gas welding flame. However, the control of the heat source and gas reaction in this process proves to be challenging [1]. The difficulty in temperature control leads to dimensional inaccuracies [2]. In contrast to conventional welding processes, gas tungsten arc welding and laser beam welding are widely used in welding sheet plates and structural applications due to their ability to produce high-quality welds through the use of a protective gas atmosphere [3]. Laser beam welding is capable of welding narrow gaps with a finer heat-affected zone [4]. Controlling welding heat input is an important issue for welding processes. Many studies in the literature focus on the microstructural changes in the heat-affected zone (HAZ) and phase transformations [5, 6].

Low-carbon sheet steels are usually hardened through cold working due to their low carbon content, which results in lower heat treatment capacity compared to their welding performance. Researchers Khamari et al. [7] are investigating the impact of tungsten inert gas (TIG) welding parameters, such as weld current, voltage, and cooling rate, on the microstructure and strength of low-carbon steels. Karadeniz et al. [8] have studied the relationship between weld penetration and welding parameters in gas metal arc welding of low-carbon sheet steels. Bendikiene et al. [9] investigate the use of monitoring and control techniques to improve the gas metal arc welding process, specifically carbon steel weldments. They explore various methods of monitoring the welding processes parameters, such as arc voltage, welding current, travel speed, and filler rod consumption.

Several studies have been conducted to optimize the weld parameters for TIG welding of low-carbon sheet steels, including the work of Essienubong and Ikechukwu. [10] who utilized experimental deflection and temperature results. Irsel [11] and Boumerzoug et al. [12] have explored the impact of grain size and microstructure of the weld zone

on the strength of TIG-welded low-carbon steels, finding that the presence of delta ferrite and Widmanstätten ferrite in the microstructure leads to increased hardness and tensile strength. Shrivastava et al. [13] investigated the effect of gas flow rate, current, and electrode gap on the strength of TIG-welded thin structures. Ebrahimi et al. [14] studied the effects of gas composition on the microstructure at GMAW (Gas Metal Arc Welding) of low-carbon steel, and Bodude and Momohjimoh [15] explored the impact of cooling rate on the microstructure of SMAW (Shielded Metal Arc Welding) low-carbon steel plates.

Since the 1950s, many studies have been conducted to improve the understanding and prediction of plastic deformation mechanisms during the heating and cooling of metals in welding processes. Welding-induced deflections and residual stresses are significant issues in structural applications, as noted by Klobcar et al. [16].

Bending, buckling, and angular distortions are common issues in welding processes due to thermally-induced residual stresses in restraint structures during the heating and cooling of weld metal [4]. The stress variation is unstable at the end of the cooling process, resulting in higher residual tensile stresses in the weld line and compressive stresses near it. These problems can be reduced with the proper selection of design and process parameters for thin-walled structures [17]. Welding residual stresses have a significant impact on the vibration responses and buckling of thin plates. Several studies have been conducted to examine the effect of welding and boundary conditions on the modal analysis of sheet steels [18]. The initial stiffness of the plate is affected by welding residual stresses. Macanhan et al. [19] found that the natural frequencies are generally decreased after a longitudinal welding process due to increasing compressive residual stresses. Conversely, vertical welds increase the structure's natural frequencies [20]. Prestressed based on residual compressive stress also plays a crucial role in the modal characteristics of structures. Increasing prestressed leads to an overall increase in the natural frequency of structures in structural applications [21].

The numerical methods, especially FEM (Finite Element Method) are commonly preferred for a better understanding of the complex nature of welding, welding distortions and welding residual stresses [17]. Thermal elastoplastic FEM models based on heat source theories and elastic FEM-based inherent strain theories are common approaches for predicting welding distortions [22]. Taylor et al. [23] used computer fluid dynamics-based heat transfer

models for predicting the temperature field at the weld fusion zone. It is aimed at finding a more reasonable approach to weld pool geometry by using thermo-fluid models. Thermomechanical modelling of welded plates is performed by many researchers after a good approximation of temperature field and heat input models. Gauss distributed heat source model defined by Friedmann is given precise results at the weld pool [24]. Goldak et al. [25] proposed a semi-elliptical model for welding heat sources, including the arc stiffness effects. This model applies to the finite element method with a moving heat source approach considering the effects of welding speed, heat input and arc length [26]. Deng [27] applied a moving heat source model with a Goldak approach to better understand the effects of the phase transition at low and medium-carbon sheet steel welding. Klobcar et al. [16] applied and verified the Sabapathy heat source model with a comparison Goldak double ellipsoid model at weld surfacing of hot worked tool steels. Chen et al. [28] studied the butt welding of low carbon sheet steels with a Goldak heat source model implementing element birth and death effects for accurate prediction of failure behaviour of the weld zone. Yona et al. [29] investigated the line heating bending of low carbon sheet steels by using Gauss heat distribution model-based Fem analysis.

At weld heating processes of sheet steels, weld currents are chosen lower for controlled weld line-affected bending. The number of the weld line pass and weld parameter optimization is determined according to these thermomechanical effects. The optimization processes are generally developed with supplementary FEM-based models with a moving heat source approach [29, 30]. Studies on the effects of weld heat input on the mechanical characteristics of low-carbon steels often focus on one of two main aspects: microstructural analysis, mechanical characterization or modal analysis tests.

In this study, the effects of heat input on microstructure, mechanical characterization, and natural frequency variations in low-carbon steels have been evaluated together. The study aims to determine whether TIG-welded vertical line heated plates, which are well-known, are suitable for use in structural applications.

To achieve this aim, the study investigates the weld heat effects on microstructure and their influence on mechanical characteristics. Additionally, it examines the macrostructural aspects through residual stress-based modal analysis results for two different boundary conditions. The effects of weld heat input are evaluated at two different stages. At the first stage the weld heat input effects on mechanical properties, plate deflection and the microstructural effects are evaluated together. In the second stage the weld heat input effects on plate are evaluated at macrostructural perspective by residual stress analysis and modal analysis considering weld heated structure mechanical properties. Despite St37 being a well-known material there is a lack of comprehensive studies in the literature that investigate the effects of weld heat input at both the micro and macro scales.

The study focuses solely on the effects of weld heat, while weld filler and weld groove effects are not considered for the sake of simplification.

2. Material and methods

In this study, the surface of St37-2 (EN10025-

2:2019) steel test specimens were exposed to welding heat using the Gas Tungsten Arc (GTA) method. The mechanical properties and microhardness of the specimens were subsequently measured. The regions of distortion in the test specimens were analyzed using both the finite element analysis method and the Coordinate Measuring Machine (CMM). SEM and optical microscope images of the specimens were also taken.

2.1. Experimental setup

The study utilized a Lincoln Invertec® water-cooled V205-T AC/DC TIG welding machine and a welding robot to apply the desired heat input to the center of St37-2 test specimens [31]. The test specimens, which measured 300 mm x 200 mm x 3 mm, were partially restrained in a simply supported form at the corners, as shown in Fig. 1.



Fig. 1 The TIG welding process fixture and welded specimen

In this research, the effect of heat input under two different welding speeds is primarily investigated. The welding parameters are presented in Table 1. The specimens underwent stationary cooling conditions at room temperature after the welding process was completed.

2.2. The mechanical properties of welded and non-welded specimens

The mechanical properties of welded and non-welded specimens were evaluated through tensile tests on five samples. Results indicate that the non-welded specimens failed at the midpoint, while the welded specimens exhibited fracture in a region far from the heat-affected zone. Notably, no cracks were observed in the heat-affected zones.

The strength and elongation ratio of welded specimens were found to be lower compared to the non-welded samples seen in Table 2, due to the grain coarsening at fusion region.

The ductility of the parts was observed to vary depending on the welding speed and current level. Specifically, the lowest elongation was achieved at lower welding speeds and higher weld currents. The fracture observed in Fig. 2 can be attributed to the microstructure in the fusion zone, which exhibited the lowest elongation.

Table 1

The weld heat input parameters in experiments

Specimen	Welding current, A	Welding voltage, V	Welding speed, mm/min	Torch distance, mm	Weld efficiency, η	Total power, W
1	100	14	300	2	0.7	980
2	100	14	200	2	0.7	980
3	125	15	300	2	0.7	1312
4	125	15	200	2	0.7	1312
5	140	15.6	300	2	0.7	1534
6	140	15.6	200	2	0.7	1534

Table 2

The mechanical properties of welded and non-welded samples

Specimen	Welding current, A	Welding voltage, V	Welding speed, mm/min	Yield strength, MPa	Tensile Strength, MPa	Elongation at break, %
1	100	14	300	299	401	24.61
2	100	14	200	314	396	23.60
3	125	15	300	310	401	24.85
4	125	15	200	328	419	23.94
5	140	15.6	300	307	404	25.60
6	140	15.6	200	331	419	22.35
7	-	-	-	344	442	30.20

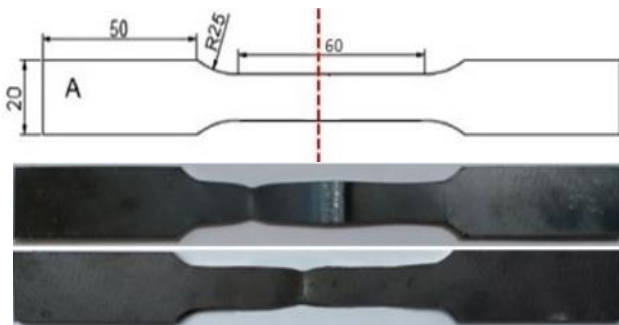


Fig. 2 Broken parts of welded and non-welded specimens

3. Result and discussion

3.1. Experimental deflection results

The experimental deflections were measured using a coordinate measurement machine (CMM) at the midpoint of the plate width. The results are presented in Fig. 3.

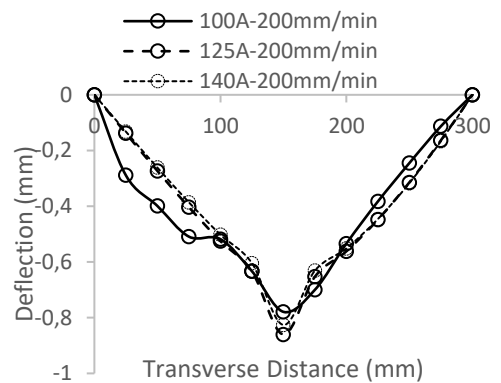
The experimental deflection values indicated an increase in deflection with higher weld input and higher weld speeds, under the given restraint conditions. These results were consistent with the findings of the tensile tests, which revealed that ductility decreased at lower weld speeds compared to higher speeds.

3.2. Microstructure investigation

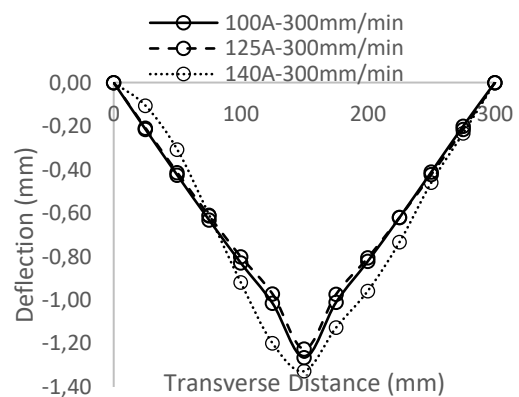
The microstructural investigation of both TIG-welded and non-welded specimens was performed in this study. Fig. 4 shows the microstructure of the non-welded specimen, which is characterized by an average grain size of 12 μm and contains ferrite and perlite phases [34].

The presence of weld gaps at the fusion and HAZ zone was not observed. It can be seen that larger grains are present in the fusion region compared to the HAZ region as the heat input increases. The microstructure in the fusion

zone differs from that in the HAZ zone due to the effects of heat input (Fig.5).



a



b

Fig. 3 Experimental deflection values for partially restraint edges: a – deflection values for 200 mm/min weld speed, b – deflection values for 300 mm/min weld speed

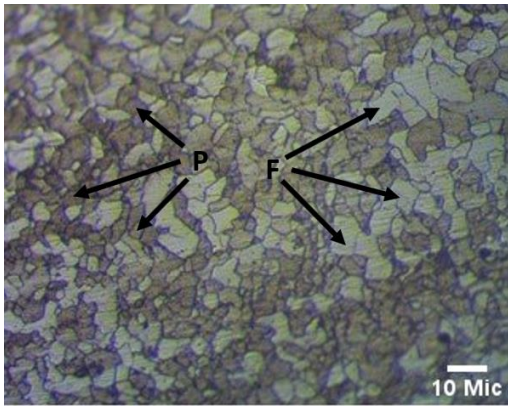


Fig.4 The microstructure of unwelded specimens

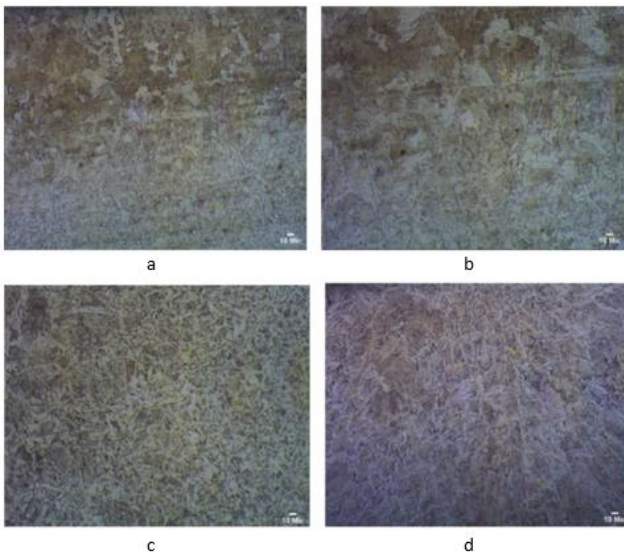


Fig 5 The microstructure of welded specimens HAZ and fusion zone: a – 140 A, 300 mm/min (5x) ITAB zone, b – 140 A, 300 mm/min (10x) fusion zone c – 140 A, 200 mm/min (5x) ITAB zone d – 140 A, 200 mm/min (5x) fusion zone

It can be observed from the figures that delta ferrite and Widmanstätten ferrite are present in the fusion and HAZ zones for decreasing weld speed. Both the microstructure shown in the figures and tensile test results indicates that the fusion zone microstructure affects ductility and creates a blocked zone for plastic deformation at lower weld speeds and higher heat inputs. The grains in the HAZ zone were analysed using Scanning Electron Microscopy (Fig. 6).

The figures indicate that recrystallization occurred in the HAZ zone for the 100 A 300 mm/min weld parameters, whereas it did not occur for the 200 mm/min weld speed due to the weld heat duration. The average grain size was found to be 7 μm and 10.5 μm for the 300 mm/min and 200 mm/min weld speeds, respectively, at the 100 A weld heat current.

3.3. Microhardness measurements at weld heat-affected zone

After polishing and sanding, the hardness samples were etched, and HV1 Vickers microhardness measurements were taken from ten different points using the Microbul-1000-DN microhardness tester. The distance between indentations is 25 mm at the microhardness measu-

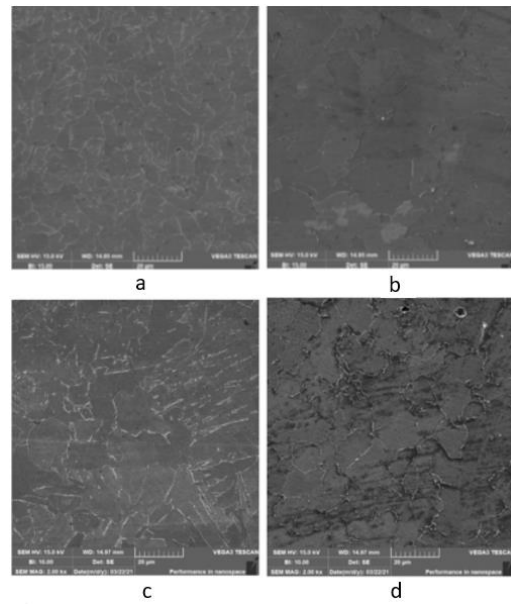


Fig. 6 The grains of welded samples at HAZ Zone a – 100 A, 300 mm/m b – 100 A, 200 mm/min c – 140A, 300 mm/min d – 140A, 200 mm/min

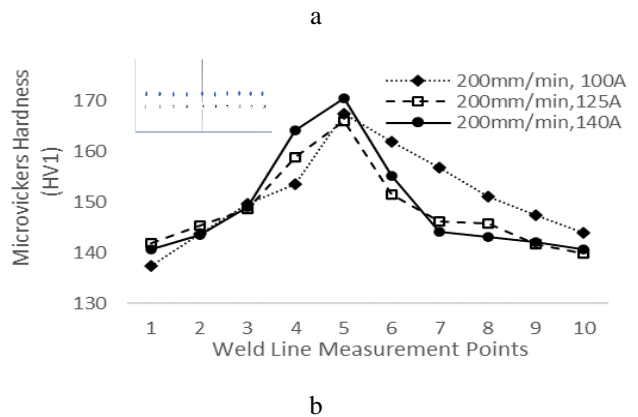
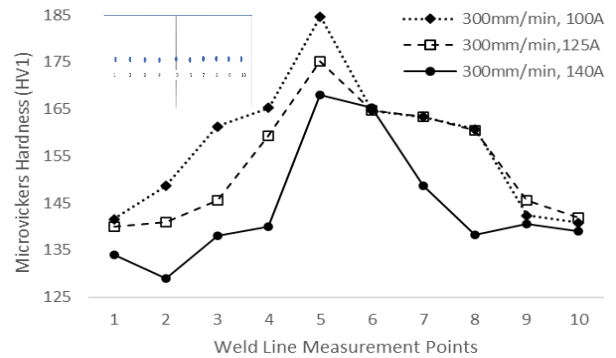


Fig. 7 Microhardness (HV1) measurements: a – 200 mm/min weld speed, b – 300 mm/min weld speed

rements. The measured points are given at the Fig. 7. The average hardness of the St32- 2 base metal was measured at 135 HV1.

When examining the hardness results, the highest value of 185 HV1 was obtained in the weld area for a current value of 100 A and a welding speed of 300 mm/min due to the recrystallized grain sizes. The hardness value of the welding and heat-affected zones was higher than the base metal hardness of 135 HV1. The fusion zone of the welding

was harder than the HAZ region due to the predominant delta ferrite phase microstructure observed in optical images.

The relationship between grain size and microhardness was found to be in good agreement.

To gain a better understanding of the effect of weld parameters on the heat-affected zone, thermomechanical analysis was conducted through finite element modelling.

3.4. Numerical analysis

In this study, the thermomechanical analysis of the TIG welding process was conducted using finite element modelling in numerical analysis. The objective was to investigate temperature variations and distortion effects through several field analyses. Thermal analysis boundary conditions were established based on the conditions of the TIG welding process used in the experiments, as shown in Fig. 1 and Table 3. Temperature changes resulting from the thermal analysis were used as thermal load inputs for the subsequent mechanical analysis, which also considered the effects of boundary conditions through numerical analysis.

Specifically, the Gauss heat flux technique was adapted to the finite element model for simulating the welding arc, and the Gauss heat flux parameters were obtained in the following Table 3.

Table 3

The moving heat source parameters at the numerical study

Welding speed	3.33 - 5 (mm/s)
Welding current heat radius (R)	2.8 (mm)
Welding power density (q)	39.96–55.63 (W/mm ²)
Welding time (t)	60 – 40 (s)

3.5. The Gauss heat flux

Gauss heat source density of the weld was defined by the following formula according to heat source radius [32].

$$q_s(r) = q_0 e^{-\frac{3r^2}{R^2}}, \quad (1)$$

$$q_0 = \frac{3}{\pi R^2} Q, \quad (2)$$

$$Q = \eta UI. \quad (3)$$

Here q_0 is heat source density per heat effected area, Q is total heat input, η is arc welding efficiency, U is arc welding voltage, I is arc welding current, r is the surface flux at radius, and R is welding pool radius.

Here welding power density (q) was calculated according to the total heat input per welding heat affected area.

3.6. Thermal analysis

The temperature variation resulting from TIG welding heat input was obtained by conducting a thermal analysis in the numerical model. The analysis time for the welding process (250 s) was determined based on the welding speed and cooling time. Temperature-dependent specific heat and conductivity values for St32 material were obtained from the literature [33].

For St37 material, thermal boundary conditions, including the convection coefficient value and radiation rate, were defined as 30 W/m² and 0.9, respectively, as described in [28]. The finite element model included a mesh density analysis for effective heat flux as illustrated in Fig. 8.

The heat flux density is crucial in evaluating the heat-affected zone during the welding process. As shown in the figure, the heat flux density increases with increasing mesh density. After considering heat flux density, and computational effort, the optimal element size was determined to be 3 mm.

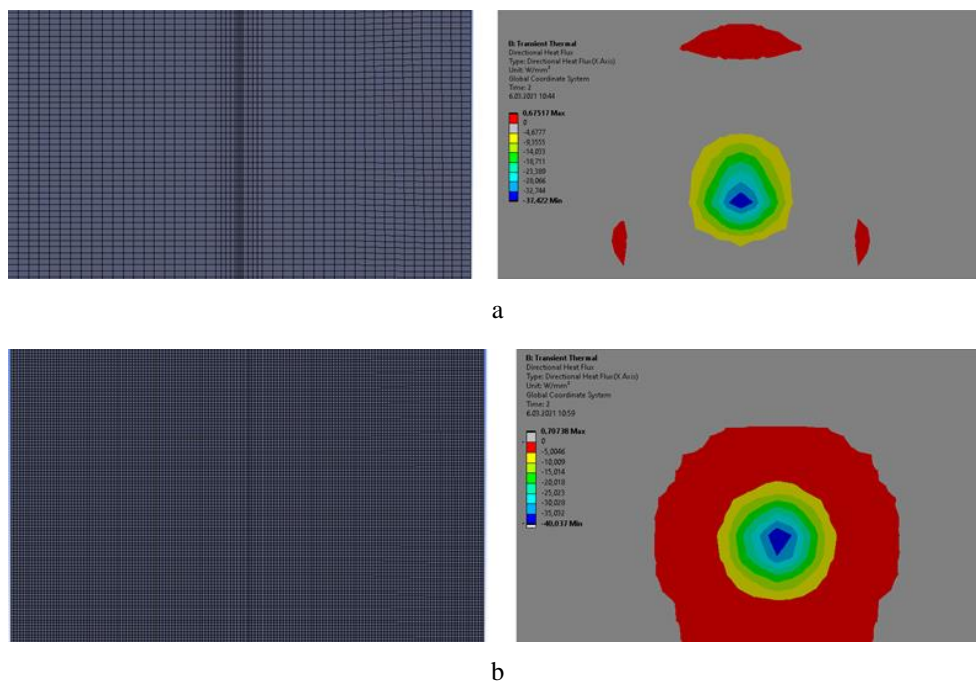


Fig. 8 The effective heat flux area at finite element model: a – 5 mm element size, b – 3 mm element size

3.7. Investigation of weld heat-affected zone

In this study, the effect of weld parameters, namely weld current and weld speed, on the weld zone was investigated. The weld heat-affected zone in experiments (EXP) was compared with the FEM analysis temperature results at the fusion zone in Fig. 9.

It is observed from the figures that the weld's ef-

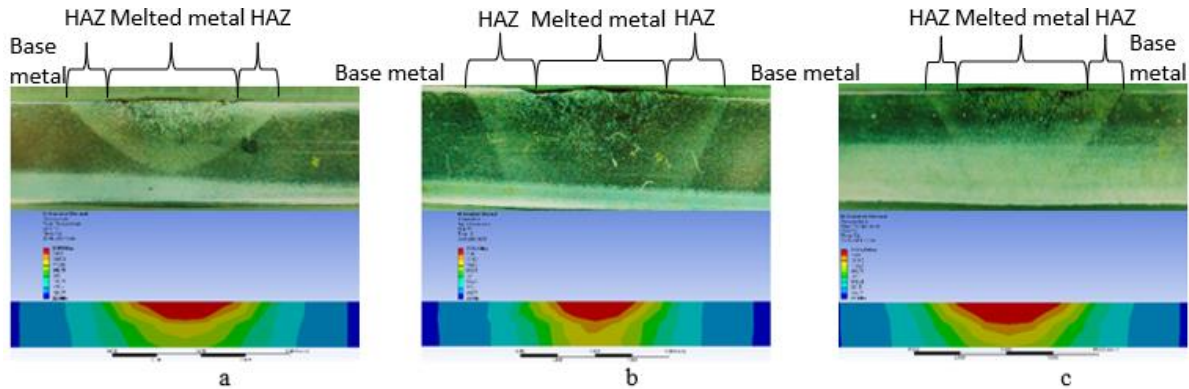


Fig. 9 The influence of weld heat in experiments: a – 125 A, 300 mm/min, b – 125 A, 200 mm/min, c – 140 A, 200 mm/min

3.8. Mechanical analysis, deflection results

The temperature-based thermal load input was used in the mechanical analysis. High deformation effects were activated by using the bilinear isotropic hardening material model in the analysis. The material properties including nonlinear effects depending on temperature were defined for St32 material [33].

The single weld line analysis was performed for

fective depth increases with higher weld current, while the weld's heat-affected width is enlarged for lower welding speed. The Gauss heat flux model used in the weld simulation accurately estimated the weld penetration.

The next section discusses the mechanical analysis, which is coupled with the thermal effects of the TIG weld line, to determine the structural effects of the TIG weld heat line.

two different boundary conditions to evaluate thermally induced deflection and residual stresses. The weld process restraints were evaluated according to stability conditions considering both experiments and finite element analysis. The model edges were restrained partially and fully in the (x, y, z) directions given in Fig. 10. It was given, namely Boundary Conditions 1 (BC1) and Boundary Conditions 2 (BC2) in the study.

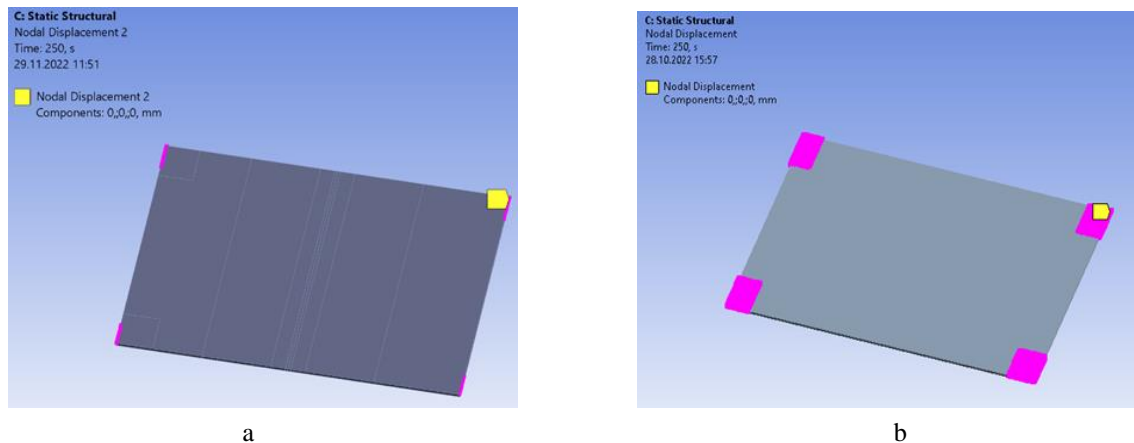


Fig. 10 The boundary conditions applied to the finite element model at the mechanical analysis: a – partially restrained edge (BC1), b – constrained at edges (BC2)

The out-of-plane deflection in the weld heat-affected zone was determined by mechanical analysis for a cooling time of 250 s, as seen in Fig. 11, for two different boundary conditions. The figure indicates that both the restraint conditions and the fusion zone affect the deflection.

The out-of-deflection results obtained by finite element analysis were compared with deflection results obtained by CMM as shown in Fig. 12. Transverse deflection effects obtained by FEM analysis are shown in Fig. 13.

The transverse deflection was enlarged for lower weld speed conditions. The out-of-deflection values for BC2 decreased due to the restraint effects and transverse de-

flections. It can be observed from the figures that the transverse deflection is highly affected at higher weld speeds for BC2 boundary conditions. The difference in deflection between 200 mm/min to 300 mm/min weld speeds is attributed to the enlargement of the heat-affected zone. As depicted in Fig. 14, transverse deflection is influenced by boundary conditions and fusion zone.

The higher compressive residual stress at the HAZ zone is believed to be the cause of this transverse deflection. A residual stress analysis was performed to gain a better understanding of the effects of boundary conditions and deflections.

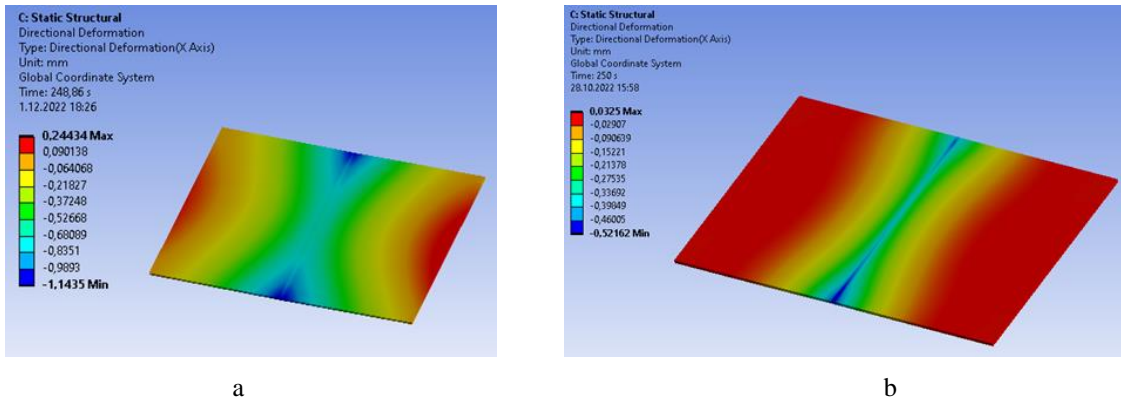


Fig. 11 The deflection analysis of TIG welded plate for (125A 300 mm/min): a – Deflection at the first model, b – Deflection at the second model

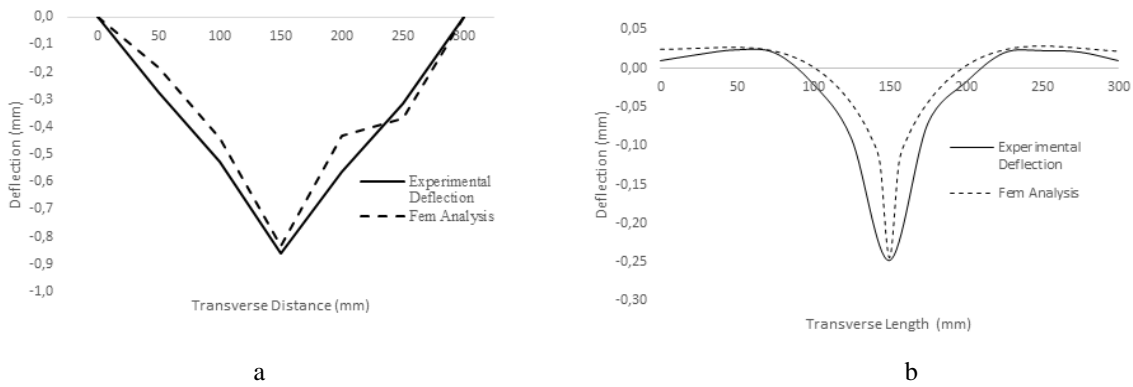


Fig. 12 Out-of-plane deflections with boundary conditions (for 125 A 200 mm/min Welding parameters): a – 125 A 200 mm/min (BC1), b – 125 A 200 mm/min (BC2)

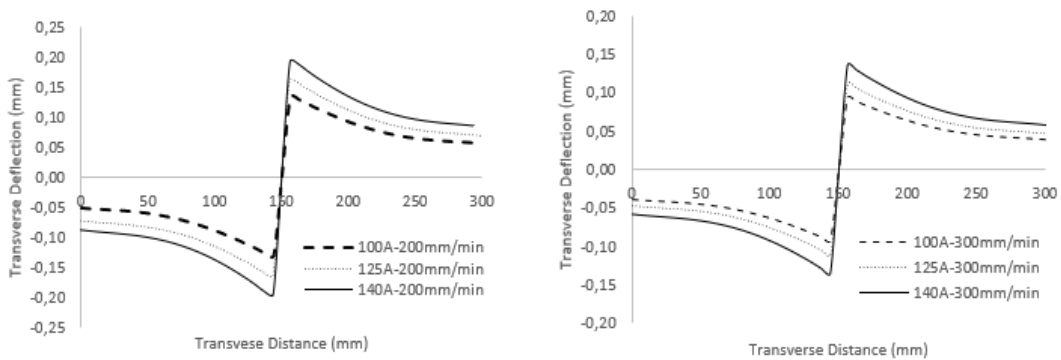


Fig. 13 The transverse deflection results of TIG welded sheet steels for (BC2)

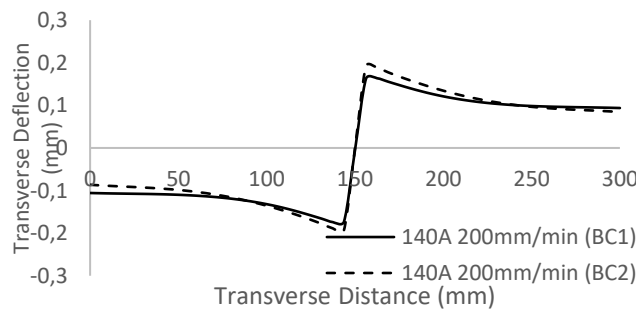


Fig. 14 The transverse deflection results of TIG welded sheet steels for 140 A 200 mm/min weld parameters

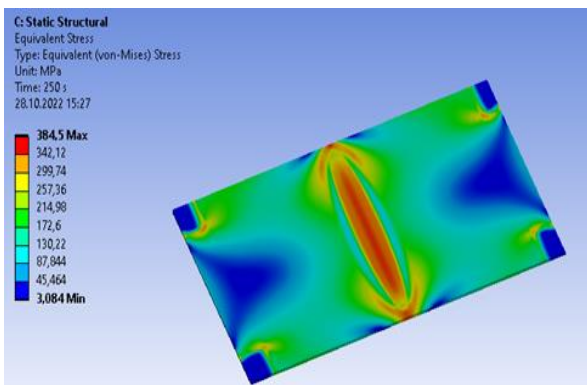
3.9. Residual stress study

Determining residual stresses is an important issue for evaluating deflection, stresses, and prestress effects in structural applications. The residual stresses were obtained by finite element models for BC2 restraint conditions given below in Fig. 15.

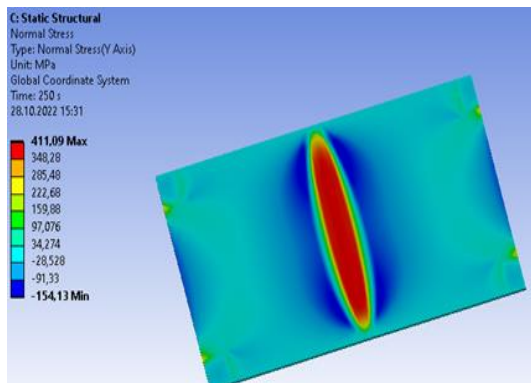
It can be observed that the von Mises yield stress values exceed the yield strength limit, causing deflection at the weld line. The distribution of residual stresses across the transverse distance reveals higher residual tensile stresses and relatively lower compressive stresses to be the main factors contributing to the deflection. The residual stress variation for BC2 boundary conditions is presented in Fig. 16.

It can be observed from the figures that the residual tensile stress values exceed the yield limit for both weld speed configurations. The stress zone is greater for lower weld speeds and increasing weld currents. The compressive stress values and their prestress effects on boundaries are higher for lower weld speeds and higher weld currents. The residual stress variation with respect to boundary conditions is evaluated in Fig. 17 for weld parameters of 100 A and 200 mm/min.

It can be observed from the figure that the weld fusion effective zone and residual stresses remain unchanged, but the compressive stresses at the boundaries are higher for BC2 restraint conditions. It is well-known that these stresses at the boundaries cause prestress in structural applications. The effects of thermally induced prestress at the boundaries were evaluated through modal analysis in this study. The

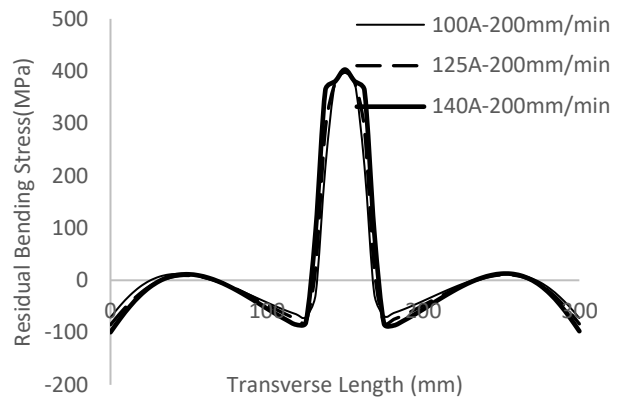


a

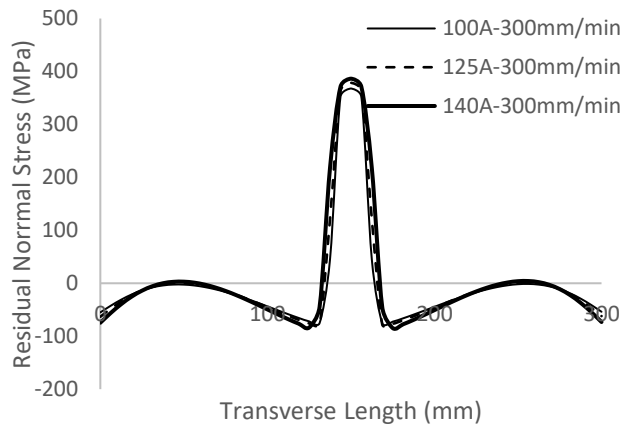


b

Fig. 15 The residual stress variation of the welded plate (125 A, 200 mm/min): a – von Mises stress, b – normal stress



a



b

Fig. 16 The residual stress variation at transverse length: a – 200 mm/min weld speed, b – 300 mm/min weld speed

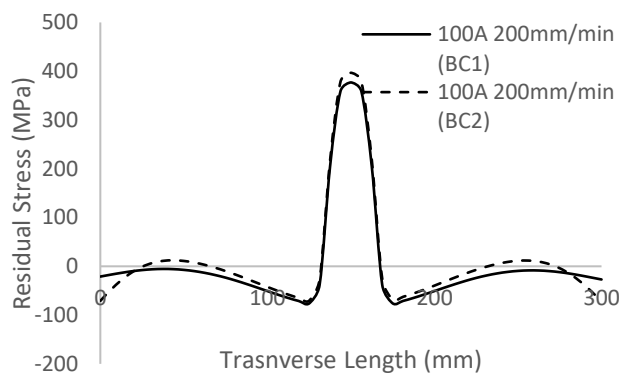


Fig. 17 The residual stress variation at transverse length for 100A 200 mm/min

couple field analysis approach was used in the study, where thermal analysis results were evaluated in the mechanical analysis, and the calculated prestress effects were used in modal analysis.

The first mode frequency results, according to boundary conditions, are provided in Table 4.

The detailed comparison of mode shapes between non-welded and welded plates is given for three modes in the following Fig. 18-19. The mode shapes of the non-welded plates are compared with those of the welded plates, taking into account the effects of prestress.

It can be observed from the table that residual compressive stresses increase with lower weld speed and higher heat inputs. The natural frequency also increases significantly due to prestressing. The maximum difference in frequency percentage between welded and non-welded specimens is observed at 140 A and 200 mm/min weld speeds. The welding and the associated thermal effects can have a significant impact on the vibration patterns assumed by the structure at higher frequencies. Additionally, the boundary

conditions imposed on the welded plates may also contribute to the observed changes in mode shapes. The mode shape results show that the mode shapes are altered due to the influence of weld heat and boundary conditions, particularly for higher modes.

A microstructural study was conducted to gain a better understanding of the thermo-mechanical effects of weld heat input.

Table 4

The boundary conditions natural frequency relation for TIG welded plates

Specimen	Welding current, A	Welding speed, mm/min	Residual compressive stresses at boundaries, MPa	Boundary Conditions	First Mode Frequency, Hz	Relative frequency percentage difference, %
1	-	-	-	BC1	103.6	-
2	-	-	-	BC2	189.9	-
3	100	200	-33.80	BC1	138.2	25.0
4	100	200	-72.22	BC2	288.8	34.2
5	100	300	-27.15	BC1	133.0	15.3
6	100	300	-53.87	BC2	258.3	21.9
7	140	200	-41.32	BC1	150.7	31.6
8	140	200	-97.37	BC2	311.2	35.2
9	140	300	-31.40	BC1	119.0	13.4
10	140	300	-73.18	BC2	283.4	28.8

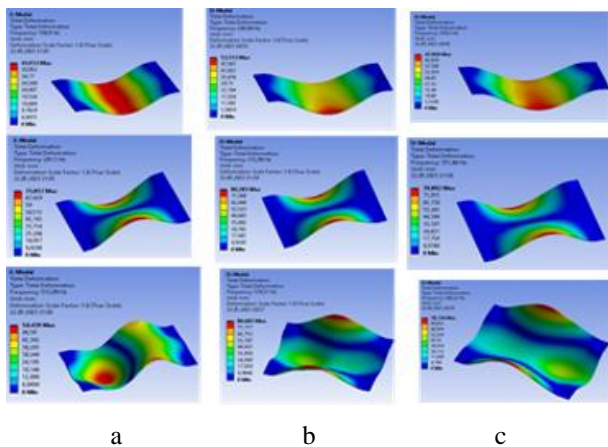


Fig. 18 Mode shape analysis for BC2: a – non-welded sample, b – 100 A, 200 mm/min, c – 100 A, 300 mm/min welded parts

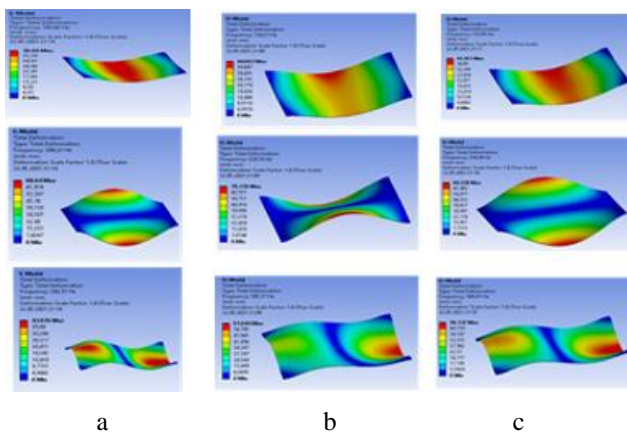


Fig. 19 Mode shape analysis for BC1: a – non-welded sample, b – 100 A, 200 mm/min, c – 100 A, 300 mm/min welded parts

4. Conclusions

This study investigates the thermomechanical effects of line heating using the TIG welding process on low-carbon steels, with a focus weld heat input. The macrostructural and microstructural aspects of weld heat input are discussed, and specimens are evaluated through tensile tests, deflection measurements and modal analysis results. The results show that higher heat input and lower weld speeds decrease ductility and increase hardness due to the microstructure of delta ferrite, Widmanstätten ferrite, and recrystallization in the fusion zone. The microstructural study sheds light on the characteristics of the weld-affected zone, which are found to be influential in the macrostructural study.

The deflection results are consistent with the tensile test results. Finite element analysis is used to investigate the macrostructural effects of weld heating. The weld heat parameters and boundary conditions are found to affect deflection and residual stresses at the weld fusion zone.

The residual stress-effective zone at the weld fusion region is enlarged for higher weld heat input and lower weld speeds seen in Fig. 16. There is a clear relationship between residual stress and the weld-affected zone in Fig. 9.

Under lower weld speed conditions in the heat-affected zone (HAZ), the out-of-plane deflection decreased, as observed in Fig. 3 and Fig. 12, and transverse deflection increased, as seen in Fig. 13. This observation aligns with the effect of weld fusion zone enlargement on the residual stress-effective zone.

The enlargement of the weld fusion zone is often associated with the development of compressive stresses near the boundaries of the weld. These compressive stresses tend to increase as a result of specific restraint edge conditions, particularly when higher weld heat input and lower weld speeds are employed, as indicated in Table 4

The increased prestress values at the boundaries due to weld heat-affected zones result in higher resonance frequencies for all vertically welded specimens, in contrast

to unwelded specimens. The maximum relative frequency percentage of 35.2% is observed for constraint edge supports when there is an increase in residual compressive stresses at boundaries due to higher weld heat input and lower weld speed.

Furthermore, the mode shape results indicate that mode shapes change as a consequence of both weld heat and boundary conditions, especially in the case of higher modes, as depicted in Fig. 18 and Fig. 19.

Overall, the results suggest that TIG welded vertical line heated plates may be suitable for use in structural applications due to their lower deflection values, higher hardness, and higher resonant frequencies. The study may be expanded to include multi-line weld heating and consider plate aspect ratios for low-carbon steels for future works.

Acknowledgments

This study was supported by Bosch Home Appliances Turkey.

References

1. **Das, B.; Biswas, P.** 2018. A review of plate forming by line heating, *J. Ship Production and Design* 34: 155-167. <https://doi.org/10.5957/JSPD.170003>.
2. **Zhang, X.; Yang, Y.; Liu, Y.** 2011. Feasibility research on application of a high frequency induction heat to line heating technology, *J. Marine Sci. Appl.* 10: 456-464. <https://doi.org/10.1007/s11804-011-1091-0>.
3. **Kadam, Y.B.** 2011. Modeling of TIG Welding Heat Source Based Steel Plate Line Heating. Master of Science Thesis, Department of Mechanical and Industrial Engineering, Indian Institute of Technology, India.
4. **Kou, S.** 2003. *Welding Metallurgy*, Second Edition. Wiley-Interscience, New Jersey. <https://doi.org/10.1002/0471434027>.
5. **Dong, H.; Hao, X.; Deng, D.** 2014. Effect of welding heat input on microstructure and mechanical properties of HSLA steel joints, *Metallurg. Microstruct. Anal.* 3: 138-146. <https://doi.org/10.1007/s13632-014-0130-z>.
6. **Lan, L.Y.; Qiu, C.L.; Zhao, D.W.; Gao, X.H.; Du, L.X.** 2012. Effect of single pass welding heat input on microstructure and hardness of submerged arc welded high strength low carbon bainitic steel, *Sci. Tech. Weld Join.* 17: 564-570. <https://doi.org/10.1179/1362171812Y.00000000048>.
7. **Khamari, B.K.; Sahu, P.K.; Biswal, B.B.** 2018. Microstructure analysis of arc welded mild steel plates. *International Conf. on Mech., Mater. And Sci. Eng.* 377, 012049. <https://doi.org/10.1088/1757-899X/377/1/012049>.
8. **Karadeniz, E.; Ozsarac, U.; Yildiz C.** 2007. The effect of process parameters on penetration in gas metal arc welding processes, *Materials and Design* 28: 649-656. <https://doi.org/10.1016/j.matdes.2005.07.014>
9. **Bendikiene, R.; Baskutis, S.; Baskutiene, J.; Kavaliauskiene, L.** 2019. Monitoring of welding process parameters in gas tungsten arc welding of carbon steel weldments, *Mechanika* 25(1): 73-81. <https://doi.org/10.5755/j01.mech.25.1.22158>.
10. **Essienubong, I.A.; Ikechukwu, O.** 2018. Optimization of TIG welding input variables for AISI 1020 low carbon steel plate using response surface methodology, *International Journal of Eng. Sci. and Application* 2(3): 114-122. Available from Internet: <https://dergipark.org.tr/en/download/article-file/543698>.
11. **Irsel, G.** 2022. Study of the microstructure and mechanical property relationships of shielded metal arc and TIG welded S235JR steel joints, *Materials Science and Engineering: A.* 830: 142320. <https://doi.org/10.1016/j.msea.2021.142320>.
12. **Boumerzoug, Z.; Derfouf, C.; Baudin, T.** 2010. Effect of welding on microstructure and mechanical properties of an industrial low carbon steel, *Engineering* 2: 502-506. <https://doi.org/10.4236/eng.2010.27066>.
13. **Shrivastava, S.P.; Vaidya S.K.; Khandelwal A.K.; Vishvakarma A.K.** 2020. Investigation of TIG welding parameters to improve strength, *Materials Today: Proceedings.* 26: 1897-1902. <https://doi.org/10.1016/j.matpr.2020.02.416>.
14. **Ebrahimnia, M.; Goodarzi, M.; Nouri, M.; Sheikhi, M.** 2009. Study of the effect of shielding gas composition on the mechanical weld properties of steel ST 37-2 in gas metal arc welding, *Materials and Design* 30: 3891-3895. <https://doi.org/10.1016/j.matdes.2009.03.031>.
15. **Bodude, M.A.; Momohjimoh, I.** 2015. Studies on effects of welding parameters on the mechanical properties of welded low-carbon steel, *J. of Minerals and Mater. Characterization and Eng.* 3: 142-153. <https://doi.org/10.4236/jmmce.2015.33017>.
16. **Klobcar, D.; Tusek, I.; Taliat, B.** 2004. Finite element modeling of GTA weld surfacing applied to hot-work tooling, *Computational Materials Science* 31: 368-378. <https://doi.org/10.1016/j.commatsci.2004.03.022>.
17. **Tsai, C.L.; Park, S.C.; Cheng, W.T.** 1999. Welding Distortion of a Thin-Plate Panel Structure, *Welding Journal* 78: 156-195.
18. **Sani, M.S.M.; Nazri N.A.; Alawi D.A.J.** 2017. Vibration analysis of resistance spot welding joint for dissimilar plate structure (mild steel 1010 and stainless steel 304). *IOP Conf. Series: Materials Sci. and Eng.* 238, 012017. <https://doi.org/10.1088/1757-899X/238/1/012017>.
19. **Macanhan, V.B.P.; Corea, E.O.; Lima A.M.G.** 2019. Vibration response analysis on stainless steel thin plate weldments, *The Int. J. of Advanced Manuf. Tech.* 102: 1779-1786. <https://doi.org/10.1007/s00170-019-03297-x>.
20. **Park, D.Y.; Bae S.Y.; Kim J.H.** 2018. A study on the effect of welding on natural frequencies of thin plate. *Maritime Safety International Conference.* 336-346. <https://doi.org/10.13000/JFMSE.2017.29.5.1356>.
21. **Li, J.** 2016. Effect of pre-stress on natural vibration frequency of the continuous steel beam based on Hilbert-Huang transform, *Journal of Vibroengineering* 18(5): 2818-2827. <http://dx.doi.org/10.21595/jve.2016.17076>.
22. **Seo, J.K.; Yi, M.S.; Kim S.H.; Kim B.; Kim S.J.** 2018. Welding distortion design formulae of thin-plate panel structure during the assembly process, *Ships and Offshore Structures* 13: 364-377.

- <https://doi.org/10.1080/17445302.2018.1475614>.
23. **Taylor G.A.; Hughes M.; Strusevich N.; Pericleous K.** 2002. Finite volume methods applied to the computational modelling of welding phenomena, *Applied Mathematical Modelling* 26: 311-322. [https://doi.org/10.1016/S0307-904X\(01\)00063-4](https://doi.org/10.1016/S0307-904X(01)00063-4).
 24. **Friedman, E.** 1975. Thermomechanical analysis of the welding process using the finite element method, *J. Pressure Vessel Technol.* 97: 206-213. <https://doi.org/10.1115/1.3454296>.
 25. **Goldak, J.; Chakravarti, A.; Bibby M.** 1984. A new finite element model for welding heat sources, *Metall Trans B* 15: 299-305. <https://doi.org/10.1007/BF02667333>.
 26. **Chen, B.Q.; Hashemzadeh, M.; Soares C.G.** 2014. Numerical analysis of the effects of weld parameters on distortions and residual stresses in butt welded steel plates. In: Guedes Soares, C.; Lopez Pena, F. (Eds.), *Developments in Maritime Transportation and Exploitation of Sea Resources*. Taylor & Francis Group; CRC Press. 309-320. <https://doi.org/10.1201/b15813>.
 27. **Deng, D.** 2009. FEM prediction of welding residual stress and distortion in carbon steel considering phase transformation effects, *Materials and Design* 30(2): 359-366. <https://doi.org/10.1016/j.matdes.2008.04.052>.
 28. **Chen, B.Q.; Hashemzadeh, M.; Soares C.G.** 2014. Numerical and experimental studies on temperature and distortion patterns in butt-welded plates, *Int. J. Adv. Manuf. Technol.* 72: 1121-1131. <https://doi.org/10.1007/s00170-014-5740-8>.
 29. **Yona, D.M.; Santhosh A.J.; Lemna, E.A.; Murugan, P.** 2022. Experimental investigation and process parameter optimization of sheet metal bending by line heating method, *Materials today: Proceedings* 56: 2398-2409. <https://doi.org/10.1016/j.matpr.2021.12.451>.
 30. **Zhou, B.; Han, X.; Tan, S.K.; Liu Z.C.** 2014. Study on plate forming using the line heating process of multiple-torch, *J. of Ship Prod. and Design* 30: 142-151. <https://doi.org/10.5957/jspd.2014.30.3.142>.
 31. **Can, K.; Dalmış, F.; Dalmış, İ.** 2022. Design and implementation of PLC based special purpose machine for surface coating, *Avrupa Bilim ve Teknoloji Dergisi* 33: 338-343. <https://doi.org/10.31590/ejosat.1019912>.
 32. **Fanous, I. F.; Younan, M. Y.; Wifi, A. S.** 2003. 3-D finite element modeling of the welding process using element birth and element movement techniques, *J. Pressure Vessel Technol.*, 125(2): 144-150. <https://doi.org/10.1115/1.1564070>.
 33. **Attarha, M.J.; Sattari-Far, I.** 2011. Study on welding temperature distribution in thin welded plates through experimental measurements and finite element simulation, *J. Mater Process. Technol.* 211: 688-694. <https://doi.org/10.1016/j.jmatprotec.2010.12.003>.
 34. **Kaya, Y.** 2018. An investigation of joinability of S235JR and S355JR construction steel by MAG welding method with cored wire electrode, *J. Polytechnic* 3: 597-602. <https://doi.org/10.2339/politeknik.375183>.

S. O. Eruslu, I. B. Akbulut, I. S. Dalmis

EFFECTS OF WELD HEAT INPUT ON MECHANICAL CHARACTERISTICS OF LOW CARBON SHEET STEELS

S u m m a r y

This study focuses on examining the variation in mechanical characteristics of low-carbon sheet steels when they are subjected to heat input from Tungsten Inert Gas (TIG) welding. The weld heat input parameters, such as welding speed and current, were controlled through the TIG welding process. A finite element analysis was performed to evaluate the couple field thermomechanical effects of the weld heat line, using the Gauss heat flux approach for thermal heat variation across the weld heat-affected zone. The numerical study yielded results for weld heat-affected deflection, residual stress, and modal analysis through the finite element model. It was found that the ductility decreased and hardness increased in the fusion zone, as a function of weld current and speed. The residual stresses and their zone of influence, as determined by weld line parameters, were found to be key factors affecting deflection and natural frequencies in structural aspects of low carbon sheet steels.

Keywords: TIG welding, welding heat input, finite element analysis, Gauss heat flux approach.

Received January 12, 2023

Accepted April 15, 2024



This article is an Open Access article distributed under the terms and conditions of the Creative Commons Attribution 4.0 (CC BY 4.0) License (<http://creativecommons.org/licenses/by/4.0/>).